Phase coexistence near the metal-insulator transition in a compressively strained $NdNiO_3$ film grown on $LaAlO_3$: Scanning tunneling, noise, and impedance spectroscopy studies

Ravindra Singh Bisht,* Sudeshna Samanta,† and A. K. Raychaudhuri‡

Unit for Nanoscience, Department of Condensed Matter Physics and Material Sciences, S.N. Bose National Centre for Basic Sciences, Block JD, Sector 3, Salt Lake, Kolkata 700098, India

(Received 17 November 2016; revised manuscript received 19 February 2017; published 27 March 2017)

We report an observation of phase coexistence near the metal-insulator transition (MIT) in a film of $NdNiO_3$ grown on crystalline substrate $LaAlO_3$. This was established through a combination of three techniques, namely, scanning tunneling spectroscopy, $1/f$ noise spectroscopy, and impedance spectroscopy experiments. The spatially resolved scanning tunneling spectroscopy showed that the two coexisting phases have different types of density of states (DOS) at the Fermi level. One phase showed a depleted DOS close to E_F with a small yet finite correlation gap, while the other coexisting phase showed a metal-like DOS that had no depletion. The existence of the phase separation leads to a jump in the resistance fluctuation (as seen through $1/f$ noise spectroscopy) at the transition, and, notably, the fluctuation becomes non-Gaussian when there is a phase separation even in the metallic phase. This was corroborated by the impedance spectroscopy, which showed a broad hump in capacitance at the transition region as a signature of the existence of two phases that have widely different electrical conductivities. The phase separation starts well within the metallic phase much above the transition temperature and makes the sample electronically "inhomogeneous" in nanoscopic scale close to the transition. We discuss certain scenarios that lead to such a phase separation in the general context of strongly correlated oxides.

DOI: 10.1103/PhysRevB.95.115147

I. INTRODUCTION

The metal-insulator transition (MIT) in oxides is a topic of considerable current interest despite a long tradition of investigations in this area [1–4]. In this class of systems, rare-earth nickelates ($RNiO_3$) form a special class [5–8]. $RNiO_3$ is a strongly correlated system that shows a temperature-driven first-order MIT. The MIT can be tuned by substitutional doping and oxygen stoichiometry change, static or dynamic strain, and ion irradiation [9–13]. In $RNiO_3$, when R = La, the material is metallic at all temperatures. In some cases, even in $LaNiO_3$, disorder or cationic substitution in the Ni site (like Co or Mn) can lead to a composition-driven transition from a metallic state to an insulating state [14,15]. For all other rare-earth elements (R), there exist temperature-driven MITs where the value of the transition temperature (T_{MI}) increases as the rare-earth ionic size decreases [8]. The transition to an insulating state is accompanied by the onset of antiferromagnetic spin order and also a structural transition. In recent years, the issue of MIT in $NdNiO_3$ has been revisited, particularly in strained thin films, through measurements of optical conductivity, electron spectroscopy, and x-ray absorption spectroscopy [16–18]. These investigations have shown that the transition cannot be described by either a typical Mott-Hubbard transition or a charge ordering transition, and, in reality, it may represent a convolution of both. It has been shown that the onset of the insulating state involves a transfer of charge density from Ni $3d$ to Nd $5d$, leading to opening of an energy gap [16,17].

In this paper, we report a new observation: In metallic films of $NdNiO_3$ (NNO) grown on $LaAlO_3$ (LAO) substrate (referred as NNO/LAO), two phases coexist, as observed using spatially resolved scanning tunneling spectroscopy (STS), supported by such probes as $1/f$ noise spectroscopy and impedance spectroscopy. We find that even in the metallic phase of $NdNiO_3$ ($T > T_{MI}$), as the insulating state is approached on cooling ($T \to T_{MI}$), the density of electronic states (DOS) at the Fermi level (E_F) is not spatially homogeneous and shows a depletion at pockets. Broadly, there are two phases that coexist in the film: a normal metallic phase, which has no depletion in DOS, and another phase having depletion in DOS. This observation has been enabled by the spatial resolution of STS, which is not possible to obtain in barrier-type tunneling experiments as done in the past. It is noted that the formation of nanoscopic insulating domains in $NdNiO_3$ film grown on $NdGaO_3$ has been observed using photoemission electron microscopy very recently. However, the insulating domain starts growing just below T_{MI} [19]. The coexisting phases make the material "inhomogeneous" on a nanoscopic scale (few tens of nanometers), where the two coexisting phases evolve as the temperature is lowered and the MIT is approached. We also show that this inhomogeneous behavior, as observed through the coexistence of two phases in STS, is also observed in very sensitive $1/f$ noise spectroscopy, which shows that the noise magnitude is extremely enhanced at the transition region, with a shift of spectral weight to lower frequency, and there is also an appearance of a strong non-Gaussian component. We further strengthen this claim by observation of a peak in the dielectric permittivity of the film at T_{MI} that establishes the existence of internal boundaries between phases with differing conductivities. The three observations together present a distinct view of the MIT in nickelates.

In correlated oxides like manganites, which show metallic conductivity, albeit with low value, there is clear evidence of depletion of DOS at the Fermi level (E_F), as has been observed in tunneling experiments using a barrier-type junction [20,21]. In $NdNiO_3$, a recent experiment reported depletion of DOS

*Corresponding author: ravindra.bisht@bose.res.in

†Present address: Centre for High Pressure Science & Technology Advanced Research, Shanghai 201203, P.R. China.

‡arup@bose.res.in

even in the metallic state ($T > T_{MI}$) before the insulating state sets in, with a small but clear hard gap [22]. Even in metallic $LaNiO_3$, there is evidence for depletion in DOS when the film is disordered, primarily arising from electron-electron interactions [14]. In the context of $LaNiO_3$, with Mn substitution at the Ni site, it has been shown that a hard gap, although small (∼10 meV), can open up at the MIT [23]. Thus, there is ample evidence that there can be depletion of the DOS in such correlated oxides, even in the metallic state, and as the transition to the insulating state is approached, a hard gap may open up in the DOS. There are also theoretical predictions that in correlated metals, the DOS at E_F may show depletion [24]. The present investigation adds a new dimension to this and shows that the depletion of DOS at E_F has a spatial dependence that can coexist with a normal conducting phase.

The MIT in NNO is strongly modified by the strain that is created by growing films on substrates with different lattice mismatches [10,25]. The biaxial lattice strain as produced by this method was found to be much more effective in tuning the MIT than that done by hydrostatic pressure. In the case of NNO film grown on $SrTiO_3$, if the film is fully strained, a tensile strain of ∼+2.6% stabilizes the insulating state and raises the T_{MI} to around ∼225 K [25]. In the case of films grown on LAO, the strain is compressive (though small ∼−0.5%), and the metallic state is stabilized with the T_{MI} pushed down below 150 K. We chose NNO/LAO for our experiment because the metallic state in NNO/LAO is stabilized strongly by the compressive strain, and recent optical conductivity experiments on such films have shown that the Drude peak actually gets strengthened on cooling [17]. It would therefore be interesting to observe the appearance of a phase with a depleted DOS in such a system.

II. EXPERIMENTAL

The films were made on the LAO single crystal substrate kept at 750 °C by pulsed laser deposition (PLD). A KrF ($\lambda = 240$ nm) pulsed laser with a repetition rate of 5 Hz and a well-characterized pellet was used for the deposition. The base pressure of the PLD chamber was 10^{-6} mbar, and the oxygen pressure during growth was 0.1 mbar. The film was cooled in an oxygen pressure of 1.2×10^3 mbar after deposition.

The resistivity measurement was done in four-probe geometry down to 30 K in a cryogen-free closed cycle refrigerator. The distance between the voltage pads was 200 μm. We used Cr/Au contact pads for the electrical measurement. Ultrahigh-vacuum (UHV) scanning tunneling microscopy (STM) operating at a base pressure of 10^{-10} mbar was used to perform STS by measuring the local tunneling conductance $g(=\frac{dI}{dV})$.

The resistance fluctuation (resistance noise) was recorded as a time series of voltage fluctuation $\Delta V(t)$ in a current-biased four-probe configuration. The measurement was done in a homemade setup that uses an alternating current (ac) carrier frequency and a sideband detection technique for a bandwidth of 10 mHz to 10 Hz. The details of the noise measurements and setup are given elsewhere [26–28]. At each temperature, the resistance fluctuation data were collected for ∼16 min, and about 1 million points were accumulated during that period, from which we conducted all the relevant data analysis. The data were taken by stabilizing the temperature at a given value with accuracy ±5 mK. This ensures that the fluctuation ($\Delta V(t)$) data are free from thermal drift. The spectral density of flicker noise ($1/f$ noise) and the Nyquist noise (thermal noise) were measured together using digital signal processing. The noise floor for our system was 2×10^{-20} V^2/Hz. From the digitized time series of the voltage fluctuation power spectrum, the probability density functions, as well as the second spectrum, were calculated.

In-plane impedance spectroscopy in the film was measured using an inductance (L)–capacitance (C)–resistance (R) meter in the frequency range of 40 Hz to 1 MHz and temperature range of 80 K to 300 K. To avoid stray capacitance from the connecting cables, we performed open-circuit and short-circuit compensations.

III. RESULTS

A. Thin film characterization

Figure 1(a) shows the cross-sectional scanning electron microscope (SEM) image of the film, and the measured thickness is 60 nm. From the analysis of the rocking curve as shown in Fig. 1(b), it is found that the film is strongly textured in the (100) direction, and the calculated substrate-induced strain [$\varepsilon = (d_{bulk} - d_{film})/d_{bulk}$] is near −0.5%. (The strain was calculated as a shift of the lattice constant from the bulk value.) The negative sign shows that strain is compressive in the (100) direction.

From the STM topography image in Fig. 1(c), one can see that the film is strain relaxed and broken into coherent regions (grains) ∼40 nm in size. The grains are oblate with the long axis aligned with the underlying substrate terrace axis.

B. Resistivity as a function of temperature

Resistivity (ρ) data (Fig. 2) show the transition from metallic state to insulating state. The compressive strain in the film stabilizes the metallic state, and the T_{MI} is shifted to a lower temperature (Fig. S1 of the Supplemental Material [29] data shows the derivative $\frac{d\rho}{dT}$ vs T). The change of sign in the derivative curve where $\frac{d\rho}{dT} = 0$ is taken as the T_{MI}. For the cooling curve, T_{MI} is ∼110 K, and for the heating curve, it is ∼148 K.

In the metallic state, $\rho \approx 2.5$ mΩ-cm at room temperature (RT), and the temperature coefficient of resistivity (TCR) ($\equiv \frac{d\rho}{TdT} \sim 5\times10^{-3}$/K) is positive. In metallic $LaNiO_3$ film, typically the ρ at RT is somewhat lower (0.5–0.6 mΩ-cm) with somewhat higher TCR of ∼8−10×10^{-3}/K.

C. Spatial dependence of DOS, local tunneling conductance map, and observation of coexisting phases

STS was used to probe the spatial dependence of the DOS at the Fermi level. The data were taken over a 200×200 nm area at 256 points in a 16×16 matrix. At each point, data were taken 10 times and then averaged. The temperature was kept stable during data scan, and no drift was observed. The data were taken with a constant direct current (dc) bias (for keeping the height of the tip above the substrate fixed), and a small ac

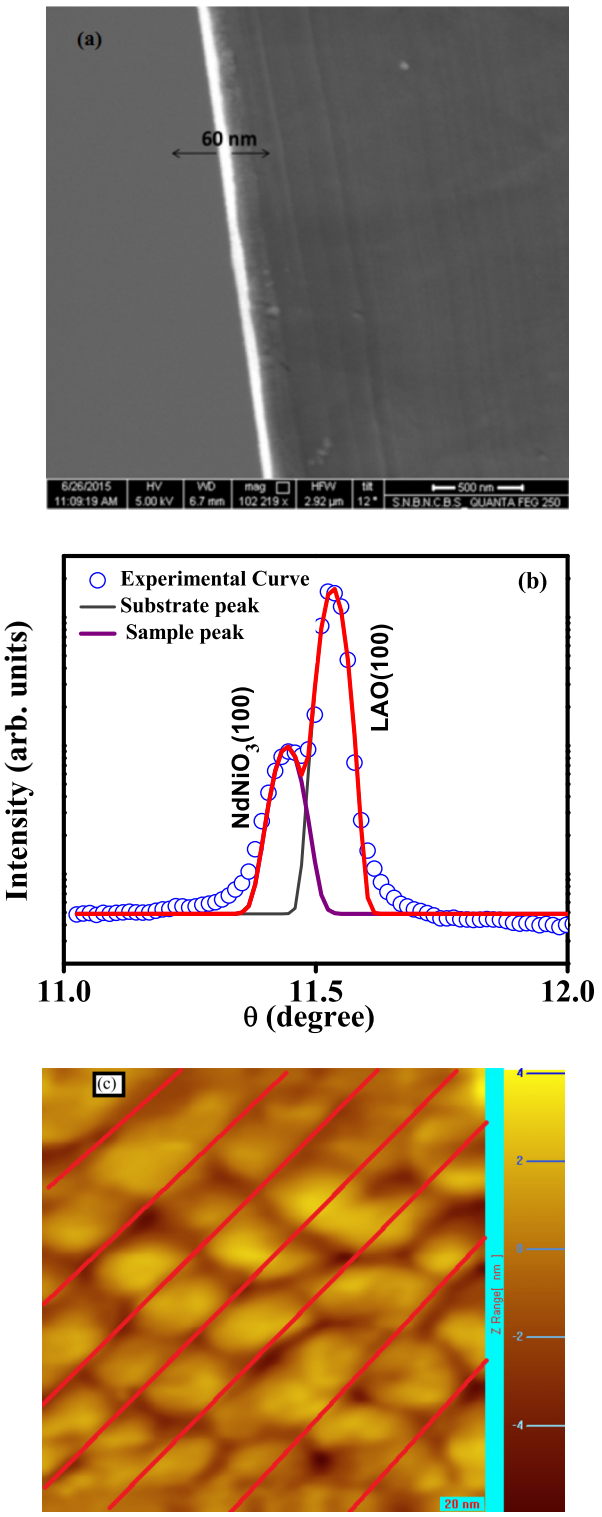

FIG. 1. (a) Cross-sectional SEM image of the film. (b) X-ray diffraction rocking curve of the $NdNiO_3$ film, where the solid curve is fitted to identify the peaks. (c) STM topography image of the film, where the red lines are guides to the eye, showing the underlying terrace pattern in which the film was grown.

modulation voltage ($\ll$ the dc bias) was used to measure the differential tunneling conductance $g = \frac{dI}{dV}$ .Taking a raster scan in the presence of an ac modulation allows one to record the topography as well spectroscopy data together. The local

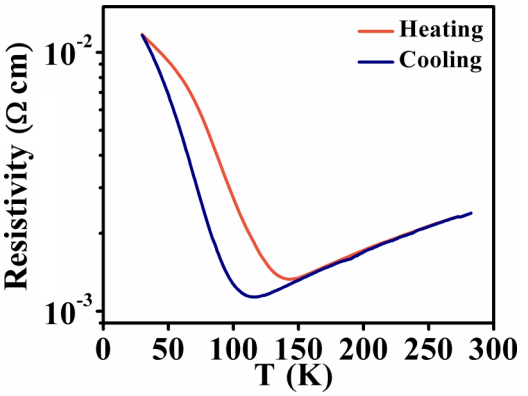

FIG. 2. Resistivity of $NdNiO_3$ film as a function of temperature during the heating and cooling cycle.

tunneling conductance map is a plot of $g = \frac{dI}{dV}$ taken at a fixed dc bias V, which defines the electron energy (=eV).

Figure 3 shows the local conductance map of NNO film grown on LAO substrate observed for a bias voltage of 0.1 V. The data are shown for two temperatures. One is close to RT (290 K), which is $\gg T_{MI}$ [Fig. 3(a)], and another is near the transition region [Fig. 3(b)]. The map is shown as a normalized tunneling conductance $\frac{g}{g_{rms}}$, where g_{rms} is defined as the root mean square (RMS) value of g taken by a spatial average of the tunneling conductances for a given bias V over the 256 points over which data are taken. This method allows us to quantify the extent of inhomogeneity that arises due to spatial dependence of DOS. At 290 K for $V = 0.1$ V, $g_{rms} = 1.36\times10^{-10}$ A/V, and g is more or less uniform, where the local value of g is within 0.8 to 1.2 of g_{rms}, although there are small local patches (dark blue) where the value of g is noticeably lower ($<0.5 g_{rms}$) and even as small as $0.3 g_{rms}$. The isolated pockets of such low g have a length scale of few tens of nanometers. The length scales over which conductance g is uniform are relatively large, and they extend over few tens of nanometer length scales.

The inhomogeneity (as measured by the spatial variation of $\frac{g}{g_{rms}}$) grows as the temperature is lowered, and closer to the transition region [T = 130 K; see Fig. 3(b)], the sample is completely inhomogeneous and mostly consists of regions of rather low g ($g_{rms} \sim 3.95\times10^{-11}$ A/V). Due to the positive TCR, the ρ at 130 K is nearly a factor of 2 lower than that at RT. However, the average tunneling conductance is lower by a factor of more than 3. Interestingly, at this temperature, there are small pockets where the local tunneling conductance is relatively high, and $\frac{g}{g_{rms}}$ is $\gg 1$. These pockets are tens of nanometers in size and are separated by regions of rather low tunneling conductance. These regions of high tunneling conductance are responsible for carrying the bulk of the conduction current, and we will see below that they are the reason for large resistance fluctuations that are non-Gaussian in nature. This coexistence of isolated metallic (high-conductance) regions separated by regions of much less conductivity also leads to the peaking of the capacitance at T_{MI}, as we will see below.

We also studied the evolution of $g - V$ as a function of temperature with spatial resolution. In Fig. 4(a), we show the temperature evolution of the $g - V$ curves at some of the marked locations. [These regions are marked by respective

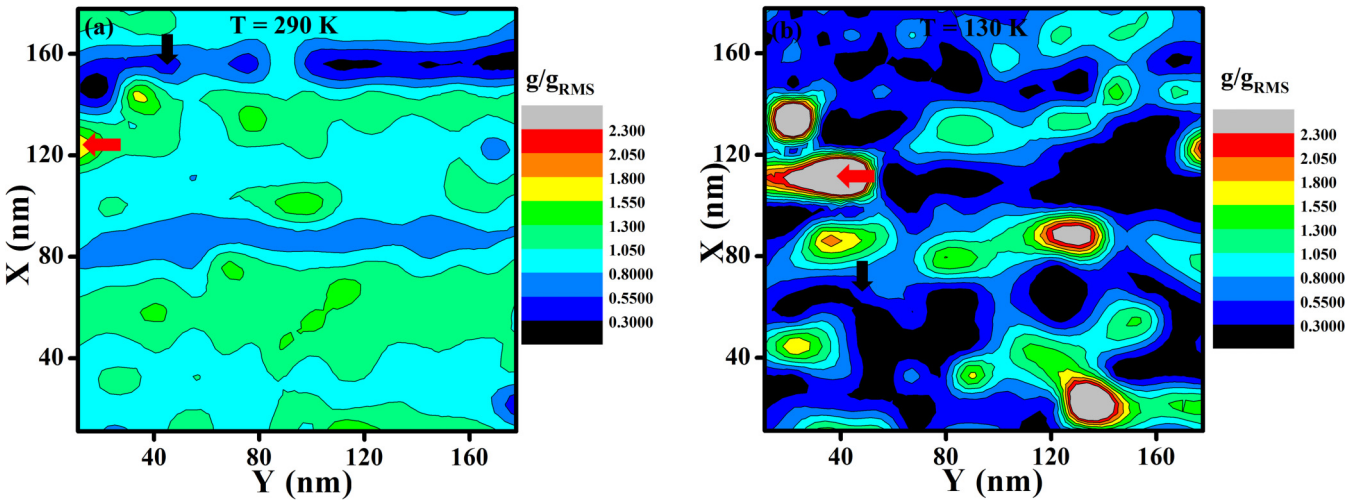

FIG. 3. Local tunneling conductance map at (a) 290 K and (b) 130 K taken in the heating cycle. The data are plotted as normalized conductance $\frac{g}{g_{\rm rms}}$. The red and black arrows show the highest and lowest g regions, respectively.

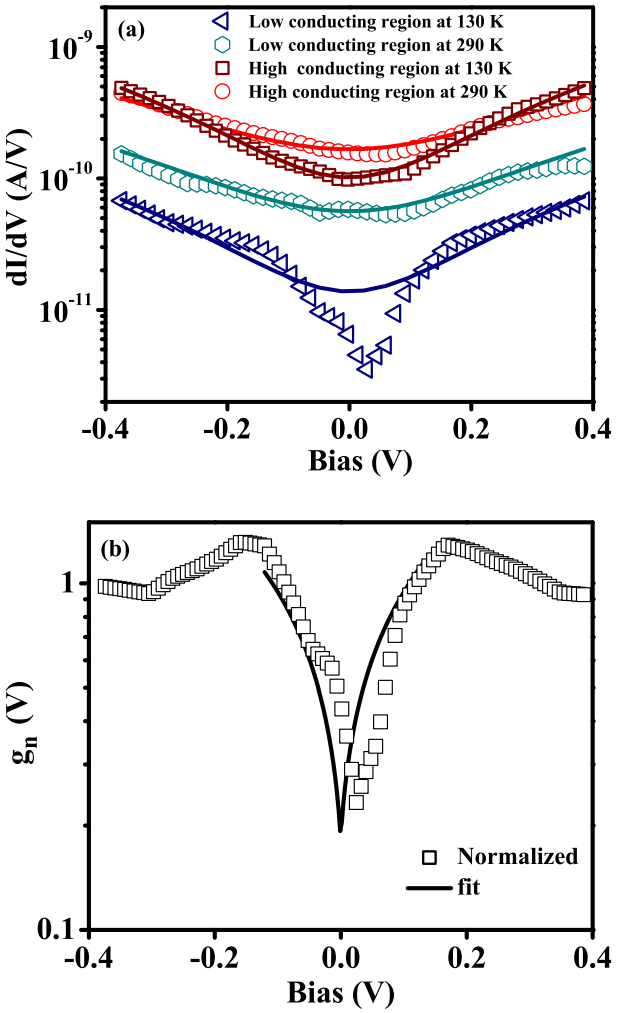

FIG. 4. (a) The bias dependence of the local tunneling conductance $g = \frac{dI}{dV}$ taken at two locations marked by arrows in Fig. 3 (solid lines show the fit to equation $g = \alpha + \beta V^2$). (b) Normalized tunneling conductance g_n as defined in the text for the region with low conductivity at 130 K.

symbols in Figs. 3(a) and 3(b).] The red (black) arrow marks the region with high (low) tunneling conductance. The regions that show very high tunneling conductance show parabolic $g - V$ curves; i.e., $g = \alpha + \beta V^2$, where α and β are constants. A parabolic $g - V$ curve is expected for a tunneling junction (with trapezoidal barrier formed by the vacuum barrier) with conventional metallic electrodes and a nearly flat DOS, as in a metal around $E_{\rm F}$ [30–32]. As shown in Fig. 4(a), $g - V$ curves in the region of high tunnel conductance remain nearly parabolic, even on cooling, although their volume fraction is decreased. In regions where the tunneling conductance is low, the $g - V$ curve is nearly parabolic at high temperatures, but on cooling, it deviates from this parabolic behavior as the DOS near the Fermi level gets depleted. This shows up as a depression in the $g - V$ curve near zero bias. To accentuate as well as quantify the deviation from the normal parabolic behavior, we plotted the normalized tunneling conductance g_n, defined as $g_n(V) = \frac{g(V)}{g_{\rm fit}(V)}$, where $g_{\rm fit}(V)$ is the fit to the tunnel conductance data for $|V| \leqslant 0.4$ V to the parabolic relation. This is shown in Fig. 4(b). For the data in the bias region $|V| < 0.2$ V, where the depletion opens up, the normalized conductance curve shows a clear dip. We find that the dip in the tunneling curve in this region fits the relation

$$g_n(V) = g_0\left[1 + \left(|V|/V^*\right)^n\right], \tag{1}$$

where the energy scale $V^* = \frac{\Delta}{e}$ is the correlation gap [15,30]. We find that at $T = 130$ K at the transition region, the fit of the data to the Eq. (1) gives the parameters $n = 0.85$ and $\Delta = 18$ eV. (The value of Δ may grow at lower temperature.)

The value of Δ near the MIT is fairly close to the value of the correlation gap (15 meV) near the MIT measured by barrier tunneling [22], and the ratio $\frac{\Delta}{k_B T_{\rm MI}} \approx 1.5$. This is much smaller than the correlation gap seen in $LaNiO_3$ at low temperatures when it undergoes a disorder-induced MIT [30]. The exponent n is less than 1 but is close to it, which has been seen in many oxides close to the critical region of MIT. In many oxides, barrier tunneling data show that as the MIT region is approached, n grows from $n = 0.5$ (expected of a DOS with

soft gap and electron-electron interaction) closer to $n = 1$ at the critical region [14,15,30]. A value of $n = 0.85$ is thus consistent with expectation from the MIT region.

The results as depicted in Figs. 3 and 4 very clearly show that there are two coexisting phases in the $NdNiO_3$ film that evolve when the temperature changes. A region with depleted DOS shows up for $T > T_{MI}$, which coexists with a metallic phase, and the depletion of the DOS is enhanced as the transition region is approached from the metallic side. Likely, these are precursor regions where the insulating phase nucleates and eventually percolates through the whole sample at the MIT.

The films used in this work are strain relaxed, and there are definite domains as seen by STM data. It will be tempting to attach the phase separation to the existence of these domains. It is quite likely that they act as nucleating centers for phase separation, but we note that there is an element of stochasticity in the formation of the phase separation. As a result, it is quite unlikely that the observed phase separation is completely determined by these domains. The size of the phase-separated regions is much larger than the size of the domains.

D. $1/f$ noise spectroscopy and the dynamic nature of phase coexistence

The STS results show that there is a phase coexistence near the MIT that consists of regions that have different tunneling conductance values. The phase with depleted DOS may evolve at $T \ll T_{MI}$ as the insulating phase, but above T_{MI}, the depletion of DOS does not automatically mean that the phase is insulating, and we refer to it as a "precursor insulator" phase.

The phase coexistence for $T > T_{MI}$ cannot be picked up easily by resistivity measurements alone because the metallic regions will carry the bulk of the current and will shunt the less conducting regions. A good probe of the electrical inhomogeneity that arises from such coexisting phases is $1/f$ noise spectroscopy, which is more sensitive than the resistivity experiment.

The observed coexistence can be static or dynamic. In dynamic phase coexistence, a conducting (insulating) region can convert to an insulating (conducting) region by crossing over an activation barrier that stabilizes the phases. This will give rise to a finite time for the dynamics to change. If that happens, one will get a resistance fluctuation that can be picked up using $1/f$ noise spectroscopy, if the time window of the noise spectroscopy is compatible with the timescale of the dynamics. The dynamic phase coexistence leading to large $1/f$ noise has been reported recently in $SmNiO_3$ as well as in VO_2 at the MIT [27,28].

From the recorded voltage fluctuation time series $\Delta V(t)$, the normalized spectral power density ($\frac{S_v(f)}{V^2}$) was calculated for the whole temperature region. The data are shown in Fig. 5(a), taken at the different temperatures. The spectral power density shows a $\frac{1}{f^\alpha}$ behavior (the solid lines represent the fit to the $\frac{1}{f^\alpha}$ behavior). The exponent α shows a clear dependence on temperature, and its value ranges from 1 to 1.4 [Fig. 5(b)].

The temperature variation of the normalized mean square resistance fluctuation ($\frac{\delta R^2}{R^2}$) is shown in Fig. 5(c). (Here, $\frac{\delta R^2}{R^2} \equiv 1/V^2 \int_{f_{min}}^{f_{max}} S_V(f)df$, where f_{min} and f_{max} define the bandwidth of measurement.) In the metallic state, $\frac{\delta R^2}{R^2}$ decreases on cooling, and the temperature variation of the fluctuation is similar to that seen in metallic $LaNiO_3$, as well as in conventional metals and alloys [33,34]. This is primarily due

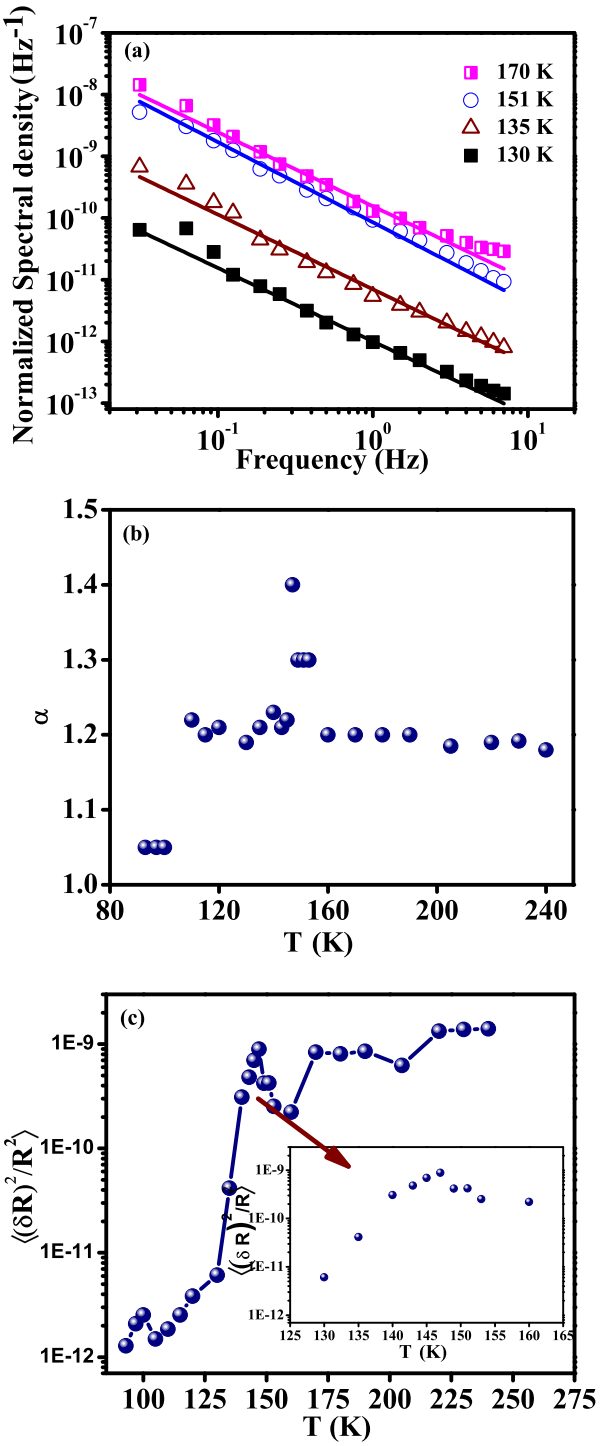

FIG. 5. (a) Normalized spectral power density of fluctuation as a function of f at different temperatures taken during the heating cycle where the solid lines represent fit to $\frac{1}{f^\alpha}$ behavior. (b) Variation of the exponent α with T. (c) Normalized mean square resistance fluctuation shown as a function of T. The inset shows the expanded part of the marked region.

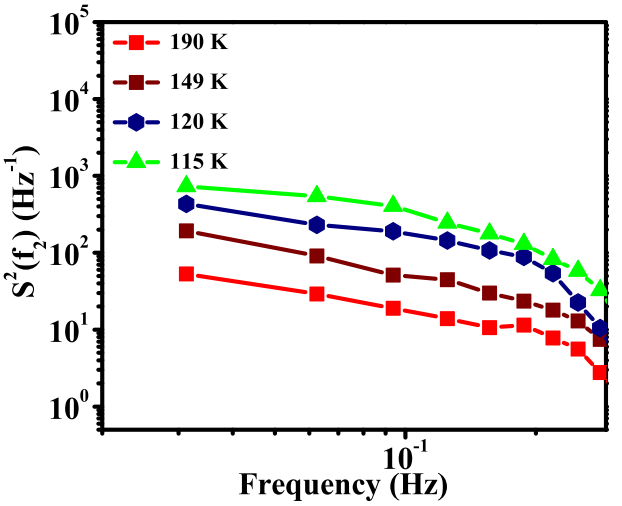

FIG. 6. Normalized second spectra $S^2(f_2)$ calculated at different temperatures.

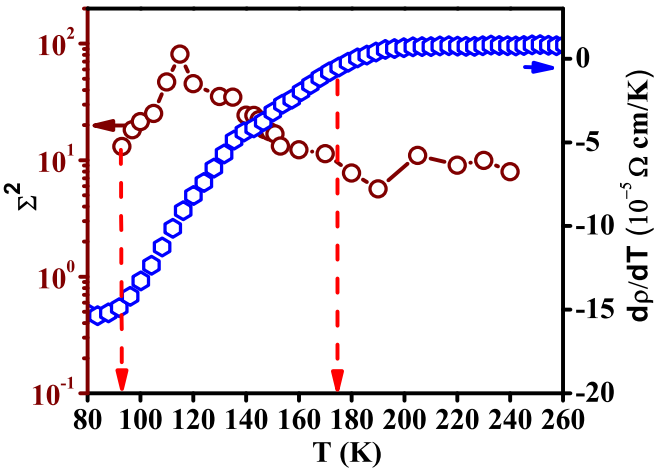

FIG. 7. Normalized variance (Σ^2) of the second spectra and $d\rho/dT$ as a function of temperature. The arrows mark the region of phase coexistence.

to the decrease in defect activation that contributes to the $1/f$ noise on cooling. However, due to an even sharper rise of R as well, $\frac{\delta R^2}{R^2}$ decreases further below $T_{\rm MI}$. The transition region marked in Fig. 5(c) is expanded and shown in the inset. It can be seen that in the transition region around $T \approx 148$ K, there is a rise in $\frac{\delta R^2}{R^2}$ over the small temperature range of 130 K to 149 K. The sharp rise occurring in the transition region is a clear signature of phase coexistence. This is similar to that seen in the region of MIT in $SmNiO_3$ and VO_2 [27,28]. We also note that there is a sharp rise in α in the same region where the resistance fluctuation also shows a clear jump. In general, in $\frac{1}{f^\alpha}$ noise in solids, the exponent α is generally ≤ 1.2 when the fluctuation predominantly arises from activated lattice defects that act as electron scattering centers. The sudden rise of α in the transition region would mean that there is a spectral shift of fluctuation in the low-frequency region. This can be also seen in Fig. 5(a), which shows the shift for the data at two temperatures (130 K and 135 K) close to the transition.

We find that the resistance fluctuation becomes strongly non-Gaussian at the transition region ($T \sim T_{\rm MI}$), where there is a sharp rise in the fluctuation. To establish the non-Gaussian behavior, we calculated the second spectrum, which is given as:

$$S^2(f_2) = \frac{\int_0^\infty \langle \Delta V^{(2)}(t) \Delta V^{(2)}(t+\tau) \rangle \cos(2\pi f_2 \tau) d\tau}{\left[\int_{f_L}^{f_H} S_V(f_1) d f_1\right]^2}, \quad (2)$$

where f_1 and f_2 are the frequencies associated with first and second spectrum, respectively. The spectrum has been calculated within the frequency bandwidth of 0.25 Hz, where f_1 is 0.25 Hz, $f_{\rm L} = 0.25$ Hz, and $f_{\rm H} = 0.5$ Hz. In Fig. 6, we show the second spectral density $s^2(f_2)$ as a function of frequency at the different temperatures, which shows the evolution of $s^2(f_2)$ as we approach $T_{\rm MI}$. It can be seen that there is a large jump in the spectral weight as the transition is approached, and $s^2(f_2)$, which has been defined above, is normalized by the square of the first spectrum, so that for a perfect Gaussian fluctuation, it is equal to 1. A deviation from unity would measure the extent of non-Gaussian behavior. The large change in the second spectrum close to $T_{\rm MI}$ can be better appreciated from the magnitude of the integrated normalized second spectrum $\Sigma^2 = \int_0^{f_H - f_L} S^2(f_2) d f_2$.

Figure 7 shows the integrated value of second spectrum Σ^2 over the whole temperature range. There is a rise in Σ^2 of nearly 1.5 orders in the transition region. In the same graph, we also show the derivative $\frac{d\rho}{dT}$. There is a clear dependence of Σ^2 on $\frac{d\rho}{dT}$. At higher temperature $T > 180$ K (in the metallic region), where $\frac{d\rho}{dT}$ is more or less constant and positive, Σ^2 is low and also constant. For $T < 180$ K, as the transition region is approached, $\frac{d\rho}{dT}$ changes sign, and the resistance starts to change rapidly. At this range, Σ^2 shows a rapid rise and eventually at low T, $\frac{d\rho}{dT}$ starts to roll off to a high (negative) value, and Σ^2 passes through a peak and also goes to a low value. In the region marked by arrows in Fig. 7, where the relative volume fraction of two coexisting phases changes, Σ^2 shows a large value.

Figure 7 clearly establishes that the inhomogeneity, as observed in the spatially resolved tunneling spectra, also leads to coexistence of two phases with different electrical conductivities, which are picked up by the noise data as well.

The large noise, in particular, the non-Gaussian fluctuation, arises in the transition range $T \sim T_{\rm MI}$. In this temperature range, the STS data [Fig. 3(b)] show that the metallic regions (regions with large tunneling conductance) have low volume fraction and are not connected. However, they can carry large current density, and there would be a charging and discharging of the metallic islands that are separated by a phase of low conductance. This phenomenon can give rise to large noise due to charge fluctuation. The large non-Gaussian component of the fluctuation arises from the transport through a system that has such isolated metallic islands due to a correlation of the current paths that is developed by a random (and dynamic) time-dependent distribution of current paths [35,36].

E. Impedance spectroscopy

The two coexisting phases as observed in STS data will have interface regions where the charge relaxation will be

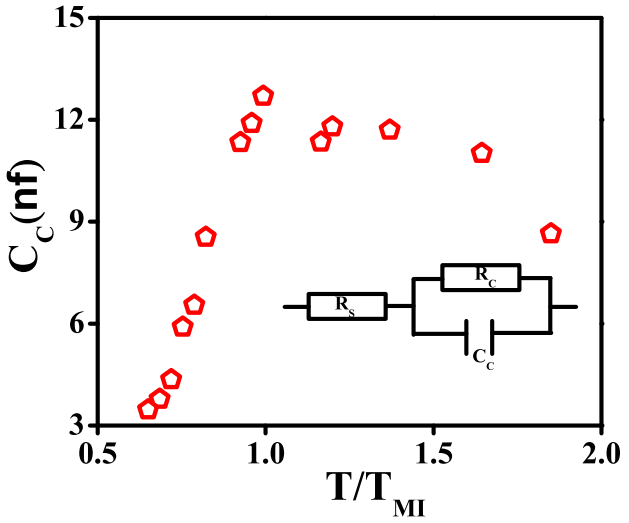

FIG. 8. Capacitance C_C as a function of T/T_{MI}.

controlled by the electrical conductivities of the surrounding regions. Closer to the transition, it may happen that regions of higher conductivities will be surrounded by regions of lower conductivities. These regions will then behave as "capacitors." It has been shown recently [37] that the existence of such internal interfaces between coexisting phases may enhance the dielectric permittivity. We carried out impedance spectroscopy to provide additional support to the observation of phase coexistence.

The detailed impedance (Z) data taken in the heating cycle [total impedance (Z) and Nyquist plot as a function of frequency and temperature] are given in Fig. S2 of the Supplemental Material [29]. The impedance data were fitted with a model using a parallel combination of R_C and C_C in series with a resistance R_S. The inset in Fig. 8 shows the model. The values of R_C,C_C, and R_S were modeled as contact resistance, stray capacitance including sample capacitance, and sample resistance, respectively. The impedance data of the film can then be given by the following relation:

$$Z(\omega) = R_S + \frac{R_C}{1 + j\omega R_C C_C}, \tag{3}$$

In Eq. (3), for $\omega \to 0$, $R_C + R_S \approx$ two-probe dc sample resistance between the leads. From the values of R_S and R_C obtained from the fit of the data at different temperatures, it was validated that it is $(R_C + R_S)$ indeed the 2-probe dc sample resistance between the leads. This is shown in Fig. S3 of the Supplemental Material [29]. The value of the capacitance C_C as a function of the scaled temperature $\frac{T}{T_{MI}}$ is shown in Fig. 8. Note that C_C shows a broad peak around $\frac{T}{T_{MI}} \approx 1$, where the resistance fluctuation ($\frac{\delta R^2}{R^2}$), as well as the second spectrum of the fluctuation (Σ^2), also shows a peak. The value of the capacitance C_C remains high even well into the metallic phase up to $\frac{T}{T_{MI}} \approx 1.6$ and then starts to go down beyond that. It is likely that at this temperature, the phase coexistence begins to appear. This is corroborated by the temperature variation of the second spectrum Σ^2 (see Fig. 7), where we observe that Σ^2 starts to rise at $T \approx 180$ K. We note that the use of impedance spectroscopy to investigate coexisting phases in a temperature-driven MIT has been reported before in VO_2 films [38,39], but not for nickelates. Furthermore, references [38,39] do not give any supporting data from complementary experiments such as STS or $1/f$ noise spectroscopy.

IV. CONCLUSION

This paper establishes that the MIT in a film $NdNiO_3$ shows phase separation at the nanoscopic scale (few tens of nanometers) and phase coexistence. This has been established through a combination of three techniques. The two coexisting phases (with nanoscopic dimensions) have a different contribution to the DOS, where one phase has depletion in DOS, and one is a normal metallic phase that has no depletion in DOS. It appears that the phase coexistence may actually start well above the MIT temperature ($\frac{T}{T_{MI}} \approx 1.5$), and the system becomes highly "inhomogeneous" electronically close to the transition temperature.

Recent theoretical developments suggest modifications in DOS in strongly correlated oxides. Predictions of a soft gap in the presence of correlation (long-range Coulomb interaction) and disorder have been known for a long time [1,2]. Relatively recently, it has been shown that a soft gap or a depleted DOS (with power-law DOS) can arise even for short-range interactions [17]. These approaches, however, do not raise the possibility of a phase separation. The possibility of interactions leading to electronic phase separation has been proposed in the context of manganites [40]. It was proposed that electrons from the conduction band can have a band-like character coexisting with carriers that are more localized polaronic in nature. The existence of strong Coulomb repulsion between the two types of electrons was shown to lead to nanoscopic phase separation. There is an apparent similarity between this picture and that observed in the STS data. The electrons in nickelates have a strong interaction with the lattice and have polaronic nature [41]. However, it is not clear at this stage whether a similar scenario or reason exists in nickelates for the observed phase separation.

Strain breaks the degeneracy of the spin-orbit and the crystal field effect determined by e_g orbitals [17,42]. The occupancy of the orbitals split by the strain would depend on the nature of the strain (compressive/tensile). It is also likely that the presence of local strain inhomogeneity can, in fact, lead to occupancy of orbitals of different type and thus different phases. While no claim can be made of the generality of this observation in the case of films other than of oxides undergoing MIT, the observation nevertheless has a generic content that may be applicable to other systems as well.

ACKNOWLEDGMENTS

The authors acknowledge the financial support from the Department of Science and Technology, India, as a sponsored Project (SR/NM/NS-53/2010) from Nanomission, Government of India. R.S.B. acknowledges Rajib Nath for his valuable suggestions in STM measurement and the technical cell of S.N. Bose National Centre for Basic Sciences for providing necessary facilities. A.K.R. acknowledges additional financial support from Science and Engineering Research Board, Government of India as a J.C. Bose Fellowship (SR/S2/JCB-17/2006).

[1] N. F. Mott, *Metal-Insulator Transition* (Taylor & Francis, London, 1990).

[2] M. Imada, A. Fujimori, and Y. Tokura, Metal-insulator transitions, Rev. Mod. Phys. **70**, 1039 (1998).

[3] Z. Yang, C. Ko, and S. Ramanathan, Oxide electronics utilizing ultrafast metal-insulator transitions, Annu. Rev. Mater. Res. **41**, 337 (2011).

[4] P. P. Edwards, R. L. Johnston, C. N. R. Rao, D. P. Tunstall, and F. Hensel, The metal-insulator-transition: A perspective, Phil. Trans. R. Soc. Lond. A **356**, 5 (1998).

[5] J. Shi, S. D. Ha, Y. Zhou, F. Schoofs, and S. Ramanathan, A correlated nickelate synaptic transistor, Nat. Commun. **4**, 2676 (2013).

[6] L. Wang, S. Dash, L. Chang, L. You, Y. Feng, X. He, K. Jin, Y. Zhou, H. Guan Ong, P. Ren, S. Wang, L. Chen, and J. Wang, Oxygen vacancy induced room-temperature metal-insulator transition in nickelate films and its potential application in photovoltaics, ACS Appl. Mater. Interfaces **8**, 9769 (2016).

[7] J. B. Torrance, P. Lacorre, A. I. Nazzal, E. J. Ansaldo, and Ch. Niedermayer, Systematic study of insulator-metal transitions in perovskites RNiO$_3$ (R = Pr,Nd,Sm,Eu) due to closing of charge-transfer gap, Phys. Rev. B **45**, 8209 (1992).

[8] G. Catalan, Progress in perovskite nickelate research, Phase Trans. **81**, 729, (2008).

[9] N. Gayathri, A. K. Raychaudhuri, X. Q. Xu, J. L. Peng, and R. L. Greene, Electronic conduction in LaNiO$_{3-\delta}$: The dependence on the oxygen stoichiometry, J. Phys.: Condens. Matter **10**, 1323 (1998).

[10] G. Catalan, R. M. Bowman, and J. M. Gregg, Metal-insulator transitions in NdNiO$_3$ thin films, Phys. Rev. B **62**, 7892 (2000).

[11] E. Mikheev, A. J. Hauser, B. Himmetoglu, N. E. Moreno, A. Janotti, C. G. Van de Walle, and S. Stemmer, Tuning bad metal and non-Fermi liquid behavior in Mott material: Rare earth nickelate thin films, Sci. Adv. **1**, e1500797 (2015).

[12] S. Heo, C. Oh, M. J. Eom, J. S. Kim, J. Ryu, J. Son, and H. M. Jang, Modulation of metal-insulator transitions by field-controlled strain in NdNiO$_3$/SrTiO$_3$/PMN-PT (001) heterostructures, Sci. Rep. **6**, 22228 (2016).

[13] Y. Kumar, R. J. Choudhary, and R. Kumar, Strain controlled systematic variation of metal-insulator transition in epitaxial NdNiO$_3$ thin films, J. Appl. Phys. **112**, 073718 (2012).

[14] A. K. Raychauduri, K. P. Rajeev, H. Srikanth, and R. Mahendiran, Low temperature studies on normal perovskite oxides: Role of correlation and disorder, Physica B **197**, 124 (1994).

[15] A. K. Raychaudhuri, K. P. Rajeev, H. Srikanth, and N. Gayathri, Metal-insulator transition in perovskite oxides: Tunneling experiments, Phys. Rev. B **51**, 7421 (1995).

[16] T. Katsufuji, Y. Okimoto, T. Arima, Y. Tokura, and J. B. Torrance, Optical spectroscopy of the metal-insulator transition in NdNiO$_3$, Phys. Rev. B **51**, 4830 (1995)

[17] M. K. Stewart, J. Liu, M. Kareev, J. Chakhalian, and D. N. Basov, Mott Physics Near the Insulator-to-Metal Transition in NdNiO$_3$, Phys. Rev. Lett. **107**, 176401 (2011).

[18] R. Jaramillo, S. D. Ha, D. M. Silevitch, and S. Ramanathan, Origins of bad metal conductivity and the insulator-metal transition in the rare-earth nickelates, Nat. Phys. **10**, 304 (2014).

[19] G. Mattoni, P. Zubko, F. Maccherozzi, A. J. H. van der Torren, D. B. Boltje, M. Hadjimichael, N. Manca, S. Catalano, M. Gibert, Y. Liu, J. Aarts, J. M. Triscone, S. S. Dhesi, and A. D. Caviglia, Striped nanoscale phase separation at the metal-insulator transition of heteroepitaxial nickelates, Nat. Commun. **7**, 13141 (2016).

[20] J. Mitra, A. K. Raychaudhuri, Y. M. Mukovskii, and D. Shulyatev, Depletion of the density of states at the Fermi level in metallic colossal magnetoresistive manganites, Phys. Rev. B **68**, 134428 (2003).

[21] J. Mitra, M. Paranjape, A. K. Raychaudhuri, N. D. Mathur, and M. G. Blamire, Temperature dependence of density of states near the Fermi level in a strain-free epitaxial film of the hole-doped manganite La$_{0.7}$Ca$_{0.3}$MnO$_3$, Phys. Rev. B **71**, 094426 (2005).

[22] S. J. Allen, A. J. Hauser, E. Mikheev, J. Y. Zhang, N. E. Moreno, J. Son, D. G. Ouellette, J. Kally, A. Kozhanov, L. Balents, and S. Stemmer, Gaps and pseudogaps in perovskite rare earth nickelates, APL Mater. **3**, 062503 (2015).

[23] D. D. Sarma, A. Chainani, S. R. Krishnakumar, E. Vescovo, C. Carbone, W. Eberhardt, O. Rader, Ch. Jung, Ch. Hellwig, W. Gudat, H. Srikanth, and A. K. Raychaudhuri, Disorder Effects in Electronic Structure of Substituted Transition Metal Compounds, Phys. Rev. Lett. **80**, 4004 (1998).

[24] H. Shinaoka and M. Imada, Soft Hubbard Gaps in Disordered Itinerant Models with Short-Range Interaction, Phys. Rev. Lett. **102**, 016404 (2009).

[25] L. Wang, S. Ju, L. You, Y. Qi, Y. Guo, P. Ren, Y. Zhou, and J. Wang, Competition between strain and dimensionality effects on the electronic phase transitions in NdNiO$_3$ films, Sci. Rep. **5**, 18707 (2015).

[26] A. Ghosh, S. Kar, A. Bid, and A. K. Raychaudhuri, A set-up for measurement of low frequency conductance fluctuation (noise) using digital signal processing techniques, arXiv:cond-mat/0402130v1.

[27] S. Samanta, A. K. Raychaudhuri, X. Zhong, and A. Gupta, Dynamic phase coexistence and non-Gaussian resistance fluctuations in VO$_2$ near the metal-insulator transition, Phys. Rev. B **92**, 195125 (2015).

[28] A. Sahoo, S. D. Ha, S. Ramanathan, and A. Ghosh, Conductivity noise study of the insulator-metal transition and phase coexistence in epitaxial samarium nickelate thin films, Phys. Rev. B **90**, 085116 (2014).

[29] See Supplemental Material at http://link.aps.org/supplemental/10.1103/PhysRevB.95.115147 for the $d\rho/dT$ as a function of temperature as well as for the detailed analysis of impedance data.

[30] A. K. Raychaudhuri, Metal-insulator transition in perovskite oxides: A low-temperature perspective, Adv. Phys. **44**, 21 (2006).

[31] A. S. Bondarenko and G. A. Ragoisha, in *Progress in Chemometrics Research*, edited by A. L. Pomerantsev (Nova Science Publishers, New York, 2005), pp. 89–102.

[32] E. L. Wolf, *Principles of Electron Tunnelling Spectroscopy* (Oxford University Press, Oxford, 1989).

[33] A. Ghosh and A. K. Raychaudhuri, Electric-field-induced migration of oxygen ions in epitaxial metallic oxide films: Non-Debye relaxation and $1/f$ noise, Phys. Rev. B **64**, 104304 (2001).

[34] A. K. Raychaudhuri, Curr. Opin. Solid State Mater. Sci. **6**, 67 (2002).

[35] S. Kar, A. K. Raychaudhuri, A. Ghosh, H. V. Lohneysen, and G. Weiss, Observation of Non-Gaussian Conductance Fluctuations at Low Temperatures in Si:P(B) at the Metal-Insulator Transition, Phys. Rev. Lett. **91**, 216603 (2003).

[36] L. M. Lust and J. Kakalios, Dynamical Percolation Model of Conductance Fluctuations in Hydrogenated Amorphous Silicon, Phys. Rev. Lett. **75**, 2192 (1995).

[37] P. Lunkenheimer, S. Krohns, S. Riegg, S. G. Ebbinghaus, A. Reller, and A. Loidl, Colossal dielectric constants in transition-metal oxides, Eur. Phys. J. Special Topics **180**, 61 (2010).

[38] J.-G. Ramırez, R. Schmidt, A. Sharoni, M. E. Gomez, I. K. Schuller, and E. J. Patino, Ultra-thin filaments revealed by the dielectric response across the metal-insulator transition in VO_2, Appl. Phys. Lett. **102**, 063110 (2013).

[39] X. Zhong, P. LeClair, S. K. Sarker, and A. Gupta, Metal-insulator transition in epitaxial VO_2 thin films on TiO_2 (100), Phys. Rev. B **86**, 094114 (2012).

[40] V. B. Shenoy, T. Gupta, H. R. Krishnamurthy, and T. V. Ramakrishnan, Coulomb Interactions and Nanoscale Electronic Inhomogeneities in Manganites, Phys. Rev. Lett. **98**, 097201 (2007).

[41] M. A. Mroginski, N. E. Massa, H. Salva, J. A. Alonso, and M. J. Martınez-Lope, Metal-insulator phase transitions of $SmNiO_3$ and $PrNiO_3$: Electrons in a polaronic medium, Phys. Rev. B **60**, 5304 (1999).

[42] I. C. Tung, P. V. Balachandran, J. Liu, B. A. Gray, E. A. Karapetrova, J. H. Lee, J. Chakhalian, M. J. Bedzyk, J. M. Rondinelli, and J. W. Freeland, Connecting bulk symmetry and orbital polarization in strained $RNiO_3$ ultrathin films, Phys. Rev. B **88**, 205112 (2013).